



Magnetic phase diagram of the two-dimensional Heisenberg spin one-half canted antiferromagnet ethyl-ammonium tetrabromocuprate(II)  
by Yadollah Hassani

A thesis submitted in partial fulfillment of the requirements for the degree of Master of Science in Physics  
Montana State University  
© Copyright by Yadollah Hassani (1988)

Abstract:

The magnetic susceptibility of  $(\text{C}_2\text{H}_5\text{NH}_3)_2\text{CuBr}_4$  has been studied as a function of an applied field (0-5500 Oe) and of temperature (1.85-120 K). The data show the antiferromagnetic ordering along b to occur at  $T_c = 10.78$  K, but the moments are canted toward the c-axis. The data in the paramagnetic region is fitted to the simple quadratic Heisenberg model. From this fit values for the exchange energy  $J/k = 18.5$  K, Curie constant,  $C = .45$  emu-K/mole, Curie-Weiss temperature,  $\theta = 37$  K and  $J/kT_c = 1.72$  have been obtained. The anisotropic exchange field,  $H_d = 2600$  G, the inter-layer exchange field,  $H_{af} = 300$  G and out of layer anisotropy field,  $H_a = 1550$  G are obtained by means of mean field calculation. The magnetic phase diagrams have been constructed along a, b, and c axes by means of susceptibility versus temperature and magnetization curves. We find the bicritical point at 10.74 K and 60 G, spin twist field,  $H_{st} = 80$  Oe, and derive the angle between the c-axis and the moment direction to be 53.2 degrees.

MAGNETIC PHASE DIAGRAM OF THE TWO-DIMENSIONAL HEISENBERG  
SPIN ONE-HALF CANTED ANTIFERROMAGNET ETHYL-AMMONIUM  
TETRABROMOCUPRATE(II)

by

Yadollah Hassani

A thesis submitted in partial fulfillment  
of the requirements for the degree

of

Master of Science

in

Physics

MONTANA STATE UNIVERSITY  
Bozeman, Montana

November 1988

Archives  
N378  
H2758  
cop. 1

APPROVAL

of a thesis submitted by

Yadollah Hassani

This thesis has been read by each member of the thesis committee and has been found to be satisfactory regarding content, English usage, format, citations, bibliographic style, and consistency, and is ready for submission to the College of Graduate Studies.

12/1/88  
Date

*Mark Winkler*  
Chairperson, Graduate Committee

Approved for the Major Department

12/1/88  
Date

*Robert J. Swan*  
Head, Major Department

Approved for the College of Graduate Studies

12/13/88  
Date

*Henry J. Parsons*  
Graduate Dean

## STATEMENT OF PERMISSION TO USE

In presenting this thesis in partial fulfillment of the requirements for a master's degree at Montana State University, I agree that the Library shall make it available to borrowers under rules of the Library. Brief quotations from this thesis are allowable without special permission, provided that accurate acknowledgment of source is made.

Permission for extensive quotation from or reproduction of this thesis may be granted by my major professor, or in his absence, by the Dean of Libraries when, in the opinion of either, the proposed use of the material is for scholarly purposes. Any copying or use of the material in this thesis for financial gain shall not be allowed without my written permission.

Signature

Hassani

Date

12/1/88

## ACKNOWLEDGEMENTS

I would like to express my sincere appreciation to all the people who contributed in making this research possible. My deepest gratitude goes to my advisor, John E. Drumheller, who guided me with continual support and encouragement. I must also acknowledge the efforts of all the others who greatly assisted me, Jerry Rubenacker, George Tuthill, Hugo Schmidt, Stuart Hutton, Donald Haines, Kenneth Emerson, and (Ravi) Ravindran. My special thanks to all the staff, faculty and my friends in the Physics Department, whom I may not have mentioned by name.

Financial support for research provided by NSF grant DMR-8702933.

## TABLE OF CONTENTS

1.	INTRODUCTION . . . . .	1
2.	THEORETICAL BEHAVIOR OF AN ANTIFERROMAGNET . . . . .	5
	Susceptibility as a Function of Temperature . . . . .	5
	Magnetization as a Function of Fields . . . . .	6
	Magnetic Phase Diagram . . . . .	9
3.	EXPERIMENTS . . . . .	17
	Sample Preparation . . . . .	17
	Crystal Structure . . . . .	17
	The Vibrating Sample Magnetometer . . . . .	18
	Powder Measurements . . . . .	20
	Coordinate System . . . . .	25
	Susceptibility Versus Temperature . . . . .	25
	Magnetization Versus Applied Field . . . . .	30
4.	MEAN FIELD CALCULATIONS . . . . .	37
	Expression for Free Energy at Zero Kelvin . . . . .	38
	Field Applied Along the Z-Axis . . . . .	45
	Field Applied Along the Y-Axis . . . . .	47
5.	MAGNETIC PHASE DIAGRAM . . . . .	54
6.	CONCLUSION. . . . .	60
7.	REFERENCES CITED. . . . .	62
8.	APPENDIX . . . . .	64

## LIST OF TABLES

Table	Page
1. Curie Temperature and Lattice Constants. . . . .	4

## LIST OF FIGURES

Figure	Page
1. The magnetic susceptibility of an antiferromagnet at zero field . . . . .	7
2. Thermal variation of molar susceptibility of an antiferromagnetic in the presence of relatively weak field . . . . .	8
3. Magnetization versus field. Field is applied perpendicular to the easy axis . . . . .	10
4. Magnetization versus applied field. Field is applied parallel to the easy axis . . . . .	11
5. Phase diagram for an antiferromagnet with small anisotropy. The external field is applied parallel to the easy axis . . . . .	12
6. The coordinate system, discussed on page 14 . . . . .	15
7. Schematic diagram of a vibrating sample magnetometer . . . . .	19
8. Temperature dependence of the molar magnetic susceptibility of powder sample at different fields . . . . .	21
9. High temperature dependence of the molar susceptibility of powder sample at $H = 4000$ Oe . . . . .	22
10. Powder susceptibility versus temperature. 1:Molecular field prediction 2:Simple quadratic Heisenberg model prediction o:Experimental data point . . . . .	23

LIST OF FIGURES-Continued

Figure	Page
11. The magnetic moment, $m$ , as a function of applied field, $H$ , at $T = 5.5$ K. The upper curve represents field along the $y$ -axis and the lower curve represents field along the $z$ -axis . . . . .	26
12. Magnetic susceptibility measured parallel to the $y$ -axis at low temperatures (circle, 10 Oe; dot, 40 Oe; plus, 100 Oe) . . . . .	27
13. Magnetic susceptibility measured parallel to the $z$ -axis at low temperatures (circle, 20 Oe; cross, 70 Oe) . . . . .	28
14. Magnetic susceptibility measured parallel to the $x$ -axis at low temperature (circle, 50 Oe; dbl.tri., 100 Oe; triangle, 150 Oe; square, 200 Oe; cross, 300 Oe) . . . . .	29
15. Magnetization versus field at 4.8 K along $x$ , $y$ , and $z$ -axes (circle, $y$ -axis; square, $x$ -axis; cross, $z$ -axis) . . . . .	31
16. Temperature dependence of weak ferromagnetic moment . . . . .	33
17. The magnetization versus applied field for several temperatures (cross, 10.5 K; dot, 6 K; square, 4.4 K; circle, 1.85 K) . . . . .	35
18. Hysteresis loop of $C_2Br$ , field is applied along the $z$ -axis . . . . .	36
19. Unit cell of $C_2Br$ , only copper ions are shown . . . . .	39
20. Spin structure for $C_2Br$ suggested by Yoshio . . . . .	40
21. Four-sublattice magnet at zero field . . . . .	42
22. Domain wall movement in soft magnet . . . . .	43
23. Spin configuration relative to the applied field . . . . .	46

LIST OF FIGURES-Continued

Figure	Page
24. Magnetization versus field fit at $T = 3.87$ K. Field applied parallel to the z-axis. The line represents the fit to the magnetization curve . . . . .	48
25. The vector $m$ shows the orientation of the resultant magnetization relative to the applied field . . . . .	49
26. Magnetization versus applied field fit at $T = 2.2$ K. Field applied parallel to the y-axis. The line represents the fit to the magnetization curve . . . . .	52
27. Calculated energy versus applied field. Field is applied along the y-axis. . . . .	53
28. Magnetic phase diagram along the y-axis . . . . .	55
29. Magnetic phase diagram along the x-axis . . . . .	57
30. Magnetic phase diagram along the z-axis . . . . .	58
31. Magnetization versus field at various temperatures, with field applied along the y-axis. (dbl.tri., 4 K; triangle, 5.5 K; circle, 6.5 K; square, 7.5 K; cross, 8.5 K) . . . . .	64
32. Magnetization versus field at various temperatures, with field applied along the y-axis. (dbl.tri., 4.4 K; triangle, 6 K; circle, 8 K) . . . . .	65
33. Magnetization versus field at various temperatures, with field applied along the y-axis. (dbl.tri., 4.79 K; triangle, 5.95 K; circle, 8.5 K) . . . . .	66
34. Magnetization versus field at various temperatures, with field applied along the y-axis. (dbl.tri., 5.25 K; triangle, 7.85 K; circle, 11 K) . . . . .	67
35. Magnetization versus field at various temperatures, with field applied along the x-axis. (dbl.tri., 4.6 K; triangle, 6.5 K; circle, 9 K; square, 10 K) . . . . .	68

LIST OF FIGURES-Continued

Figure	Page
36. Magnetization versus field at various temperatures, with field applied along the x-axis. (dbl.tri., 2.6 K; dot, 3 K; plus, 8.5 K) . . . . .	69
37. Magnetization versus field at various temperatures, with field applied along the x-axis. (circle, 4.8 K; dbl.tri., 7 K; triangle, 9.5 K; dot, 10.5 K) . . . . .	70
38. Magnetization versus field at various temperatures, with field applied along the x-axis. (circle, 2 K; dot, 3.6 K; dbl.tri., 2.6 K; triangle, 5.5 K) . . . . .	71
39. Magnetization versus field at various temperatures, with field applied along the z-axis. (dbl.tri., 5.25 K; triangle, 6.77 K; circle, 8.45 K; square, 9.7 K; cross, 11 K) . . . . .	72
40. Magnetization versus field at various temperatures, with field applied along the z-axis. (dbl.tri., 4.8 K; triangle, 5.95 K; circle, 7.6 K; square, 10.5 K) . . . . .	73

## ABSTRACT

The magnetic susceptibility of  $(C_2H_5NH_3)_2CuBr_4$  has been studied as a function of an applied field (0-5500 Oe) and of temperature (1.85-120 K). The data show the antiferromagnetic ordering along b to occur at  $T_c = 10.78$  K, but the moments are canted toward the c-axis. The data in the paramagnetic region is fitted to the simple quadratic Heisenberg model. From this fit values for the exchange energy  $J/k = 18.5$  K, Curie constant,  $C = .45$  emu-K/mole, Curie-Weiss temperature,  $\theta = 37$  K and  $J/kT_c = 1.72$  have been obtained. The anisotropic exchange field,  $H_d = 2600$  Oe, the inter-layer exchange field,  $H_{AF} = 300$  Oe and out of layer anisotropy field,  $H_a = 1550$  Oe are obtained by means of mean field calculation. The magnetic phase diagrams have been constructed along a, b, and c axes by means of susceptibility versus temperature and magnetization curves. We find the bicritical point at 10.74 K and 60 Oe, spin twist field,  $H_{ST} = 80$  Oe, and derive the angle between the c-axis and the moment direction to be 53.2 degrees.

## CHAPTER ONE

## INTRODUCTION

The purpose of this investigation is to analyze the magnetic properties of  $[\text{C}_2\text{H}_5\text{NH}_3]_2\text{CuBr}_4$  and construct magnetic phase diagrams along all three axes.  $[\text{C}_2\text{H}_5\text{NH}_3]_2\text{CuBr}_4$  is a member of the  $[\text{C}_n\text{H}_{2n+1}\text{NH}_3]_2\text{CuX}_4$  family, hereafter abbreviated as  $\text{C}_n\text{X}$  where X represents a Cl or Br atom and n varies from 1 to 10.  $\text{C}_n\text{X}$  compounds have attracted special attention because they can serve as an approximation to the ideal two dimensional spin 1/2 Heisenberg ferromagnets. In the two dimensional Heisenberg  $S = 1/2$  ideal system, exchange interactions are confined to two dimensions, and long range order above zero K cannot be sustained. However,  $\text{C}_n\text{X}$  compounds order at a temperature  $[T_c]$  between 7 K to 16 K. This series of compounds deviate from the ideal system due to the presence of a weak anisotropy and coupling in the third dimension, which in turn causes the long range ordering at a temperature higher than zero K.

Yoshio reported this compound to be a weak ferromagnet. Weak ferromagnetism occurs mainly in antiferromagnetic crystals such as  $\alpha\text{-Fe}_2\text{O}_3$ ,  $\text{NiF}_2$ ,  $\text{MnCO}_3$ , and  $\text{CoCO}_3$ . The problem of weak ferromagnetism was first studied by Dzialoshinski [2] who contributed the weak ferromagnetism to an interaction of the form  $d\circ[S_1XS_2]$ . This term represents the antisymmetric part of the spin coupling. In contrast Yoshio claims that the source of the canting is symmetrical, i.e., of the

form  $S_1 \circ K_s \circ S_2$ . This discrepancy prompted us to do further investigation on this compound. Also, we have confusing ac susceptibility data.

Although the crystal structure of  $C_nX$  compounds are similar, the magnetic behaviors of the members of this family differ from one another. For instance, the ferromagnetic layers may couple antiferromagnetically as in  $C_2Cl$  [1]. In  $C_1Cl$ , the coupling between layers is ferromagnetic [1]. On the other hand, in  $C_3Br$  a weak ferromagnetic moment appears along the c-axis [1]. The ferromagnetic intra-layer exchange constant,  $J/k$ , varies from 15.4 K for  $C_4Cl$  to 22 K for  $C_5Br$  [3]. Inter-layer interaction,  $J'/k$ , is very weak compared to that of in-plane interaction,  $J'/J=1.7 \times 10^{-3}$  for  $C_1Br$  and  $J'/J=10^{-5}$  for  $C_{10}Cl$  [4]. For  $C_2Br$ , different values of  $J'/J$  have been reported. Yoshio reports  $Z|J'|/ZJ=7 \times 10^{-4}$  where  $Z$  is the number of nearest neighbors in the plane and  $Z'$  is the number of nearest neighbors in the next plane. If we take  $Z=4$  and  $Z'=8$  then we get  $J'/J=3.5 \times 10^{-4}$ . L. de Jongh gives a value of  $1.7 \times 10^{-3}$  which is about 4.8 times larger than Yoshio's  $J'/J$  value. Although inter-layer exchange coupling is small, it plays a major role in the magnetic behavior of  $C_nX$  compounds below the transition temperature. The anisotropy field within the layer is of the order of  $10^{-5}$  to  $10^{-4}$  of the ferromagnetic exchange field. The out-of-plane anisotropy remains the same for all compounds and is of order of  $10^{-3}$  of the ferromagnetic exchange field [4].

The crystal structure of the known members of the  $C_nX$  family is orthorhombic [4], which means the axes of a unit cell are perpendicular and also  $a \neq b \neq c$ . In this series of compounds  $a$  and  $b$  are nearly equal,

but the distance between the planes increases as  $n$  is increased. Table I is taken from reference [5] where  $d_1$  is the distance between copper ions within a layer and  $d_2$  is the distance between nearest neighbor copper ions in different layers. It also shows lattice constants up to  $n=6$ . For  $C_2Br$  a transition of 10.72 K is given. We measured the transition temperature to be  $10.75 \pm 0.05$  K. Professor K. E. Emerson, of Montana State University, has measured the lattice constants of  $C_2Br$  to be  $a=7.9525$ ,  $b=7.7187$ , and  $c=21.4191$  Angstrom which is in agreement with Table 1.

The second chapter of this thesis is concerned with the theoretical behavior of antiferromagnets. Chapter Three deals with methodology, and includes a discussion of susceptibility versus temperature and field. In Chapter Four, mean field calculations are carried out and numerical values for magnetic parameters are given. Finally, in Chapter Five, magnetic phase diagrams along three axis are constructed and discussed.

Table 1: Curie temperature and lattice constants

Compound	$T_c$ (K)	$a_o$ (Å)	$b_o$ (Å)	$c_o$ (Å)	$d_1$ (Å)	$d_2$ (Å)
$C_1Cl$	8.9	7.54	7.3	18.55	5.24	9.99
$C_2Cl$	10.2	7.47	7.35	21.18	5.24	11.22
$C_3Cl$	7.61	7.65	7.33	24.66	5.29	12.89
$C_4Cl$	7.27					
$C_5Cl$	7.25	7.51	7.38	34.81	5.26	17.8
$C_6Cl$	7.65					
$C_2Br$	10.72	7.95	7.72	21.5	5.54	11.44
$C_3Br$	10.41	8.00	7.69	24.32	5.54	12.78

## CHAPTER TWO

## THEORETICAL BEHAVIOR OF ANTIFERROMAGNETS

Susceptibility as a Function of Temperature

An antiferromagnet consists of two or more magnetic sublattices. The simplest antiferromagnetic arrangement is one in which the magnetic atoms can be subdivided into two sublattices, A and B, so that moments belonging to sublattice A point in one direction, and those belonging to sublattice B point in the opposite direction. The magnetic interaction between the sublattices is such that, below the Neel temperature [ $T_N$ ], spins on the sublattice A point in a positive direction and those of sublattice B point in a negative direction, leading to zero net moment. The direction of the magnetization of each sublattice below the Neel temperature will be along the direction of the anisotropy field. This is called easy direction or easy axis.

Cooling a paramagnet in zero applied field leads to a transition from the paramagnetic to antiferromagnetic state at the Neel temperature. Above the Neel temperature, the system behaves as a paramagnetic system and obeys the Curie-Weiss law:

$$\chi = C/(T - \theta)$$

where C and  $\theta$  are called Curie constant and Curie temperature, respectively. The susceptibility below the Neel temperature along the

easy axis decreases reaching a finite value at  $T=0$ . This is illustrated in Figure 1.

In cooling a paramagnetic system, if a constant external field is applied normal to the easy axis, the applied field will produce a torque that tends to rotate the sublattice magnetization. The internal field will oppose this rotation. One can show, by molecular field calculation, that the susceptibility below the Neel temperature remains constant and assumes a value of  $C/2$  (see Figure 2).

On the other hand, if the external field is applied parallel to the easy axis, the susceptibility decreases below the Neel temperature and goes to zero at  $T=0$ , as shown in Figure 2. This is because there is a strong interaction between the moments of the two sublattices and a relatively small applied field cannot turn over the moments of the negative sublattice to the direction of the field (Figure 2).

In a powder sample in which the easy directions are distributed at random, the susceptibility is given by

$$\chi_{\text{pow}} = (1/3) \chi_{\text{pa}} + (2/3) \chi_{\text{pe}}$$

where  $\chi_{\text{pa}}$  and  $\chi_{\text{pe}}$  denote the parallel and perpendicular susceptibility, respectively, as shown in Figure 2.

#### Magnetization as a Function of Field

A magnetization curve [M vs H] yields an important feature of a magnetic system, the strength of the anisotropy field. For an antiferromagnet, we can consider two cases: field applied 1] normal to the easy axis and 2] parallel to it.

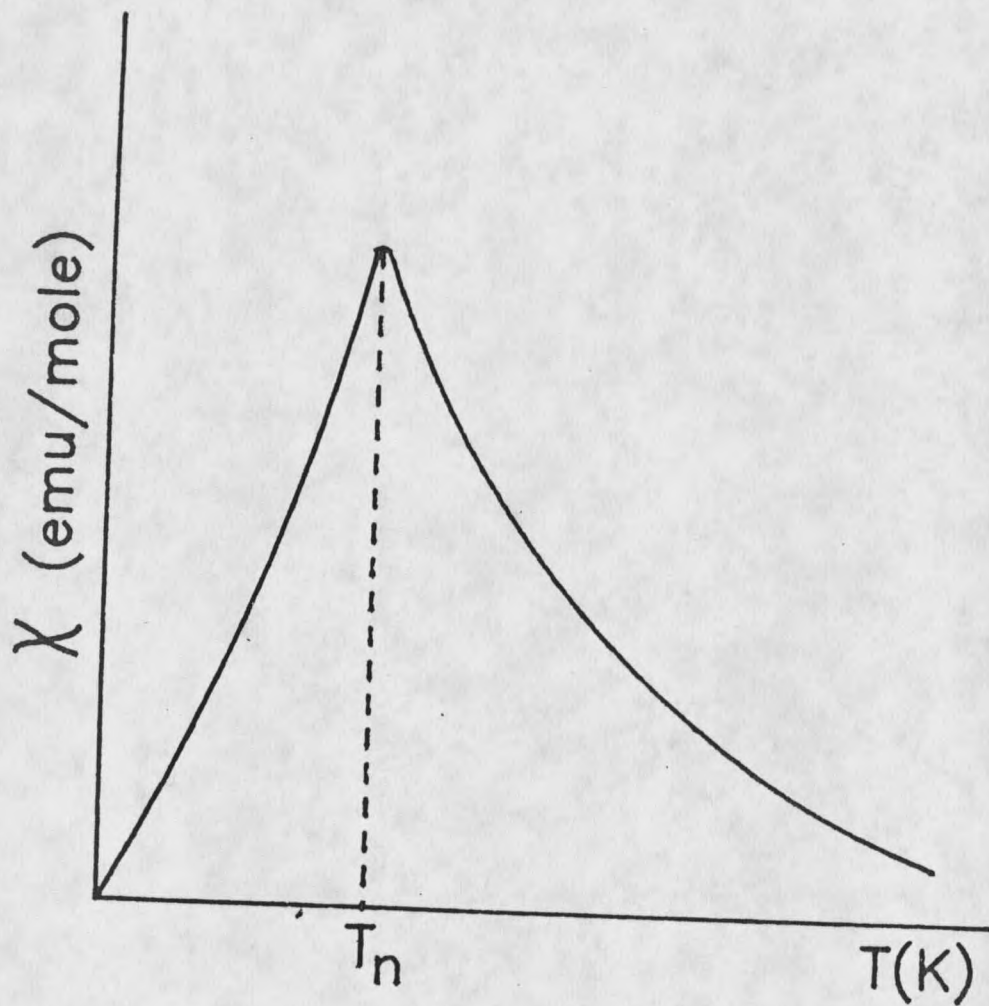


Figure 1. The magnetic susceptibility of an antiferromagnet at zero field

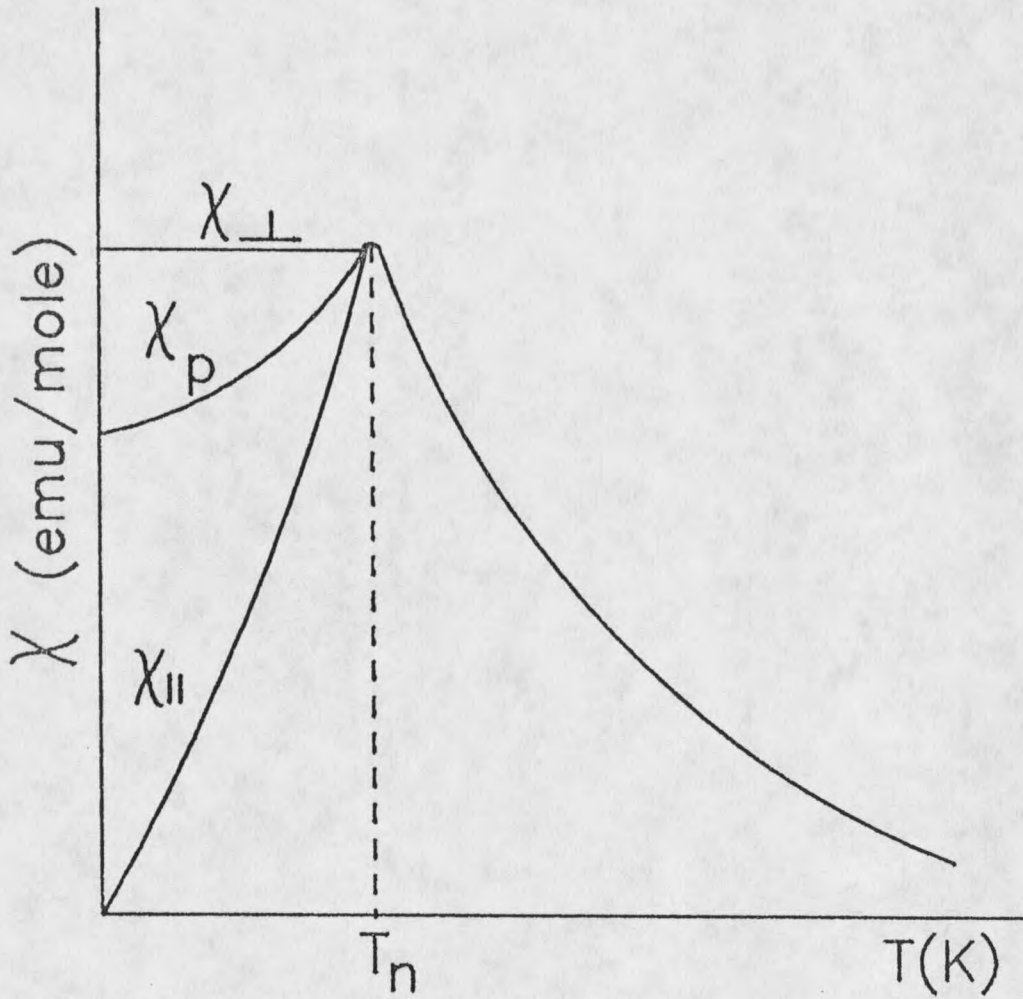


Figure 2. Thermal variation of molar susceptibility of an antiferromagnetic in the presence of relatively weak field

1] Field normal to easy axis: an increasing applied field,  $H$ , will turn each sublattice magnetization away from the easy axis and tends to align it in the direction of the applied field. As field is increased, magnetization will increase linearly until saturation is achieved. This gives the magnetization versus field curve shown in Figure 3.

2] Field parallel to easy axis: for a field applied in the direction of the easy axis, the applied field will be resisted by the anisotropy field until the applied field equals that of the anisotropy field. This field is called spin-flop field. At the spin-flop field two sublattice magnetization will reorient themselves such that they are perpendicular to the direction of the applied field. As the field is increased further, magnetization will increase linearly as a function of the applied field until saturation is achieved. This is shown in Figure 4.

We will show that, below some critical temperature, an antiferromagnetic ordering develops in  $C_2Br$ . In contrast to the usual antiferromagnets, the magnetization vectors of the sublattices are not exactly antiparallel to each other, but are inclined at some angle. In  $C_2Br$  spin-flop does not occur. However, a spin rearrangement occurs, which we will call a spin-twist transition.

#### Magnetic Phase Diagram

A magnetic phase diagram [ $H_a$  vs  $T$ ] can be constructed for an ordered system to illustrate the phases that occur. A hypothetical phase diagram for an antiferromagnet when small anisotropy with the external field applied parallel to the easy axis is shown in Figure 5.

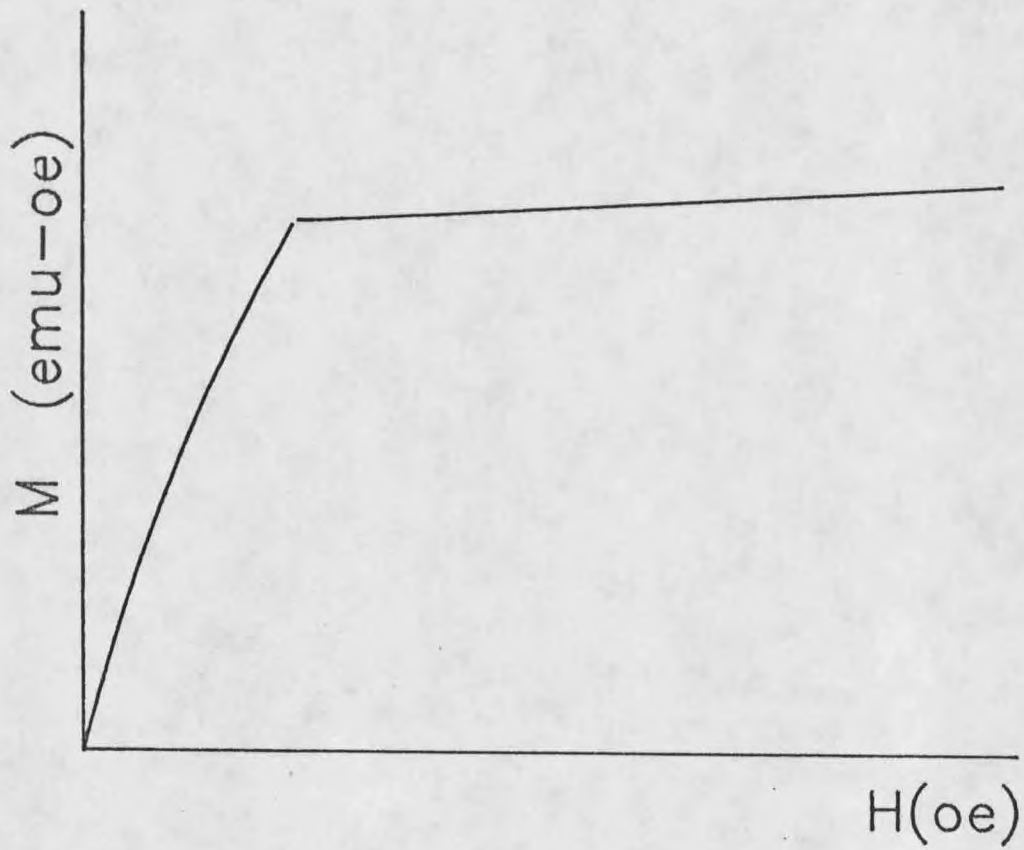


Figure 3. Magnetization versus field. Field is applied perpendicular to the easy axis

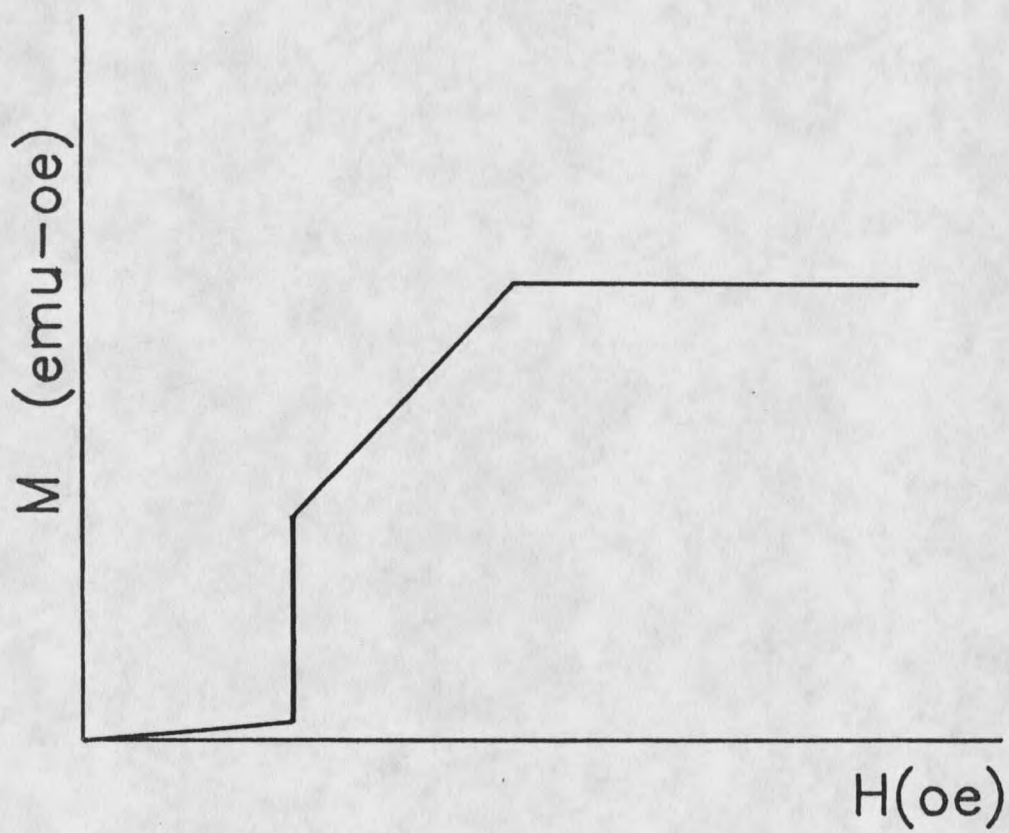


Figure 4. Magnetization versus field. Field is applied parallel to the easy axis

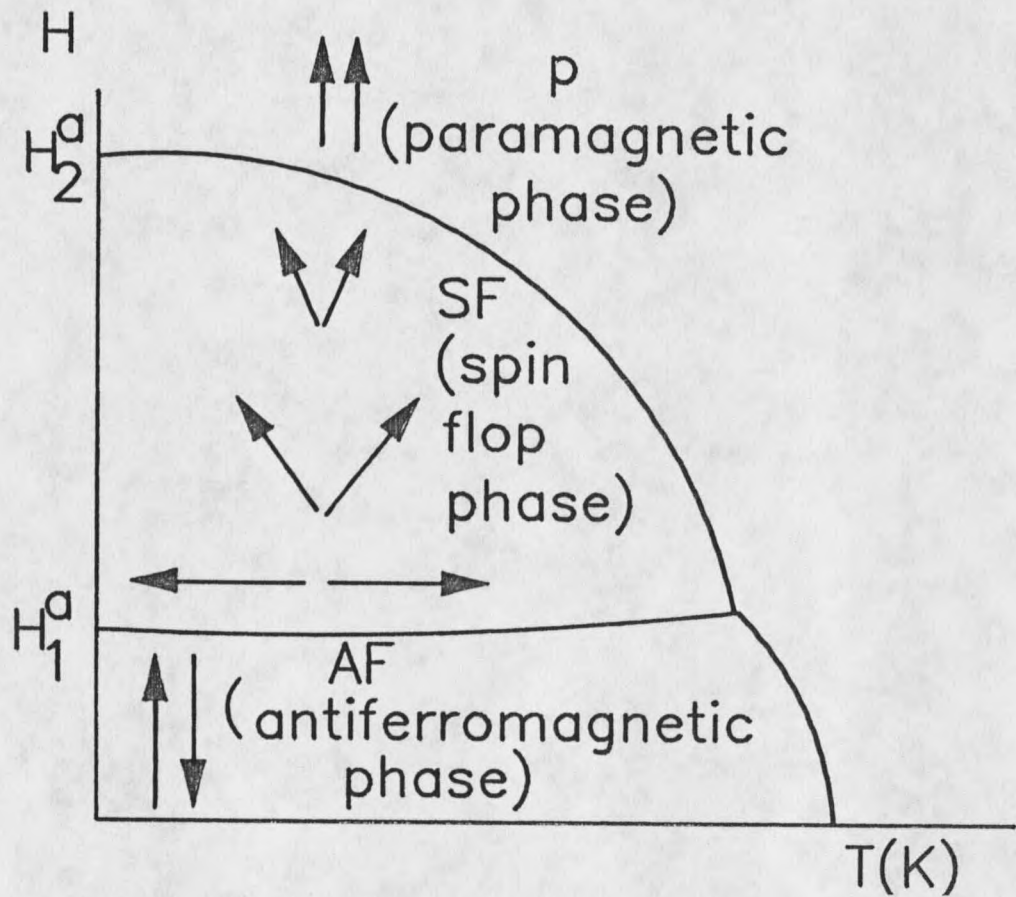


Figure 5. Phase diagram for an antiferromagnet with small anisotropy. The external field is applied parallel to the easy axis

This figure illustrates three distinct phase boundaries. These are: 1] paramagnetic [P] to antiferromagnetic [AF]; 2] AF to spin-flop [SF]; and 3] SF to P phase boundaries. When a field is applied along the easy axis of an antiferromagnet, a competition is set up between the applied field and the internal field, causing  $T_c[H_a]$  to drop to a lower value as  $H_a$  increases. This is a second order phase transition and forms the P-AF phase boundary.

If an increasing field is applied, at a constant temperature below the Neel temperature, along the easy axis of an antiferromagnet, nothing will happen until the applied field becomes equal to that of anisotropy field. When the applied field slightly exceeds the anisotropy field, the moments flop [nearly] perpendicular to the direction of the field. The field at which moments flop, is called spin-flop field. The transition is first order and this is a thermodynamically favored state. This forms the AF-SF phase boundary. A second order transition occurs when the moments line up with the field and the system enters into a paramagnetic state [SF-P transition].

Next we will derive the zero-T critical field by the method of mean field calculation and follow closely the format given by Drumheller, Raffaele, and Baldwin (6).

The spin-Hamiltonian for a two-sublattice antiferromagnet can be written

$$H = -g\mu_B H \cdot S_i + 2J \sum S_i \cdot S_j + LS_{iz}^2. \quad (1)$$

The first term is the Zeeman term. The second term represents the antiferromagnetic interaction between  $S_i$  and  $S_j$ . The exchange energy,

$J$ , is assumed to be positive. The third term indicates the  $z$ -axis is the hard axis. We will subdivide the lattice of magnetic atoms into two sublattices, A and B, such that sublattices A and B point in opposite directions. According to the molecular field theory all magnetic atoms are identical and equivalent and  $S_k$  can be replaced by its average value  $\langle S \rangle$ . Then the energy of Equation (1) can be written:

$$E = - (1/2) g\mu_B H \langle S_A \rangle - (1/2) g\mu_B H \langle S_B \rangle + Jn \langle S_A \rangle \langle S_B \rangle + L \langle S_z^2 \rangle \quad (2)$$

where  $n$  is the number of the nearest neighbor ions. We will use the coordinate system shown in Figure 6. The angle between sublattice spins and the hard axis ( $z$ -axis) is defined as  $\theta$ . Energy for the AF phase, from Equation (2) is

$$E_{AF} = - JnS^2, \quad (3)$$

For simplicity, we have written  $S$  for  $\langle S \rangle$ . For the spin flop phase, Equation (2) becomes

$$E_{SF} = - g\mu_B HS \sin\theta - JnS^2 \cos 2\theta + LS^2 \cos^2 \theta \quad (4)$$

since  $E_{SF}$  is a function of  $\theta$ , it can be minimized by setting  $dE/d\theta = 0$ . This gives

$$\sin\theta = g\mu_B HS / (4JnS^2 - 2LS^2). \quad (5)$$

From Equation (5)  $\cos\theta$  and  $\cos 2\theta$  can be found. Substituting these into Equation (4) will result in

$$E_{SF} = [-(g\mu_B HS)^2 - 8(JnS^2)^2 - 4(LS^2)^2 + 12(LS^2)(JnS^2)] / 4(2JnS^2 - LS^2) \quad (6)$$

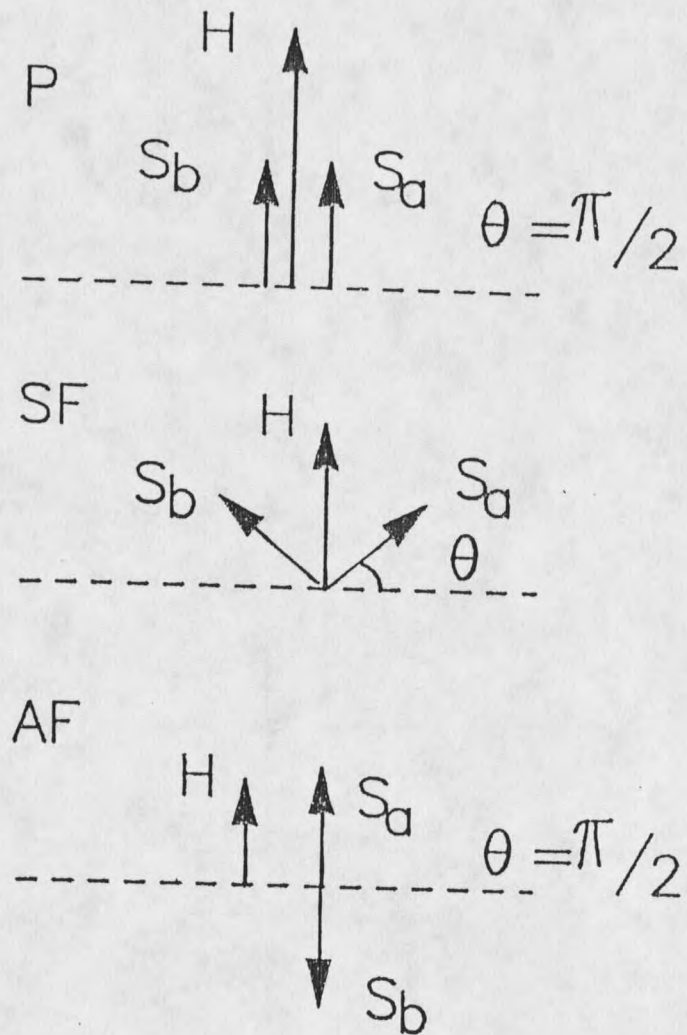


Figure 6. The coordinate system, discussed on page 14

At the spin-flop transition, Equations (6) and (3) are equal. This gives

$$(g\mu_B HS)^2 = 4[(2LS^2)(JnS^2) - (LS^2)^2], \quad (7)$$

dividing Equation (7) by  $(g\mu_B s)^2$ , results in

$$H^2 = 2(2nJS/g\mu_B) (2LS/g\mu_B) - (2LS/g\mu_B)^2. \quad (8)$$

We define  $H_{AF} = (2nJ/g\mu_B)$  and  $H_A = (2LS/g\mu_B)$  and relabel  $H$  as  $H_{SF}$ , then Equation (8) becomes

$$H_{SF} = [2H_{AF}H_a - H_a^2]^{1/2}, \quad (9)$$

$H_{SF}$  is the value of the antiferromagnetic to spin-flop transition field extrapolated to zero K. The field of the spin-flop to paramagnetic transition can be obtained by replacing  $\theta$  by  $\pi/2$  in Equation (5), this yields

$$H_c = 2H_{AF} - H_a. \quad (10)$$

These equations or appropriately similar ones will be used for our analysis in Chapter 5.

## CHAPTER THREE

## EXPERIMENTS

Sample Preparation

The  $(C_2H_5NH_3)_2CuBr_4$  crystals were prepared by Professor K. E. Emerson of Montana State University. The ratio of the mole weight of  $C_2H_5NH_3Br$  and  $CuBr_2$  is two to one. Two parts of  $C_2H_5NH_3Br$  and one part of  $CuBr_2$  were dissolved in alcohol. The solution was filtered and put in a closed beaker in the presence of ether. By this method, good single crystals of fairly thin plates were obtained.

Crystal Structure

Although the crystal structure of  $(C_2H_5NH_3)_2CuBr_4$  has not been solved in detail, dimensions of the unit cell and the distance between the copper-copper within the layer and between neighboring layers are known (Table 1). The crystal structure of known compounds of the  $(C_nH_{2n+1}NH_3)_2CuX_4$  series are all orthorhombic with space group  $P_{bca}$ . These compounds consist of nearly isolated magnetic sheets of  $CuX_4$  ( $X = Cl$  or  $Br$ ), which are separated by two sheets of alkyl-ammonium groups. The cell constants  $a$ ,  $b$ , and  $c$  for  $C_2Br$  are 7.9525, 7.7187, and 21.4191 Angstrom, respectively (7). Preliminary studies of this compound have shown that the unit cell is orthorhombic and the space group is  $P_{bca}$  (7).

### The Vibrating Sample Magnetometer

Data were obtained using an EGG PAR Model 155 magnetometer. In addition to the magnetometer console and head, the system includes an electromagnet with field control and a cryostat with temperature control and measurement. The system is interfaced to an Apple II computer.

A schematic of the magnetometer head is shown in Figure 7 (8). It consists of the following: a mechanical vibrator, a long rod, a magnet, pick up coils, and a capacitor plate assembly. The sample is attached to the end of a long rod and placed between the pole faces of the magnet. The rod and the sample are vibrated perpendicular to the applied field by the mechanical vibrator at a frequency of 82.5 hertz. The magnetization of the sample induces a voltage in pick up coils placed on the magnet pole faces. The induced voltage has a frequency of 82.5 hertz and an amplitude proportional to the magnetization of the sample and to the amplitude of the vibration (9). The purpose of the capacitor is so that the detected voltage can be made independent of vibrational amplitude. A nickel standard is used to calibrate the magnetometer, since the saturation magnetization of nickel is known.

Temperatures over a range of 1.7 K to room temperature were controlled by both a current heater mounted below the sample and an adjustable gaseous flow rate. Temperatures at the lowest range were obtained by pumping on the sample chamber. The temperature was measured with a carbon glass resistor mounted directly above the

















































































































